Electronic Supplementary Information

The Slow Magnetic Relaxation Regulated by Ligand Conformation of A Lanthanide Single-Ion Magnet [HexN][Dy(DBM)$_4$]

Wen-Bin Sun,[a, b] Bing Yan,[a] Yi-Quan Zhang,[a] Bing-Wu Wang,*[a] Zhe-Ming Wang,[a] Jun-Hua Jia[a] and Song Gao*[a]

[a] Beijing National Laboratory of Molecular Science State Key Laboratory of Rare Earth Materials Chemistry and Applications, College of Chemistry and Molecular Engineering, Peking University Beijing 100871, China.

[b] Key Laboratory of Functional Inorganic Material Chemistry Ministry of Education, Heilongjiang University, Harbin 150080, China.

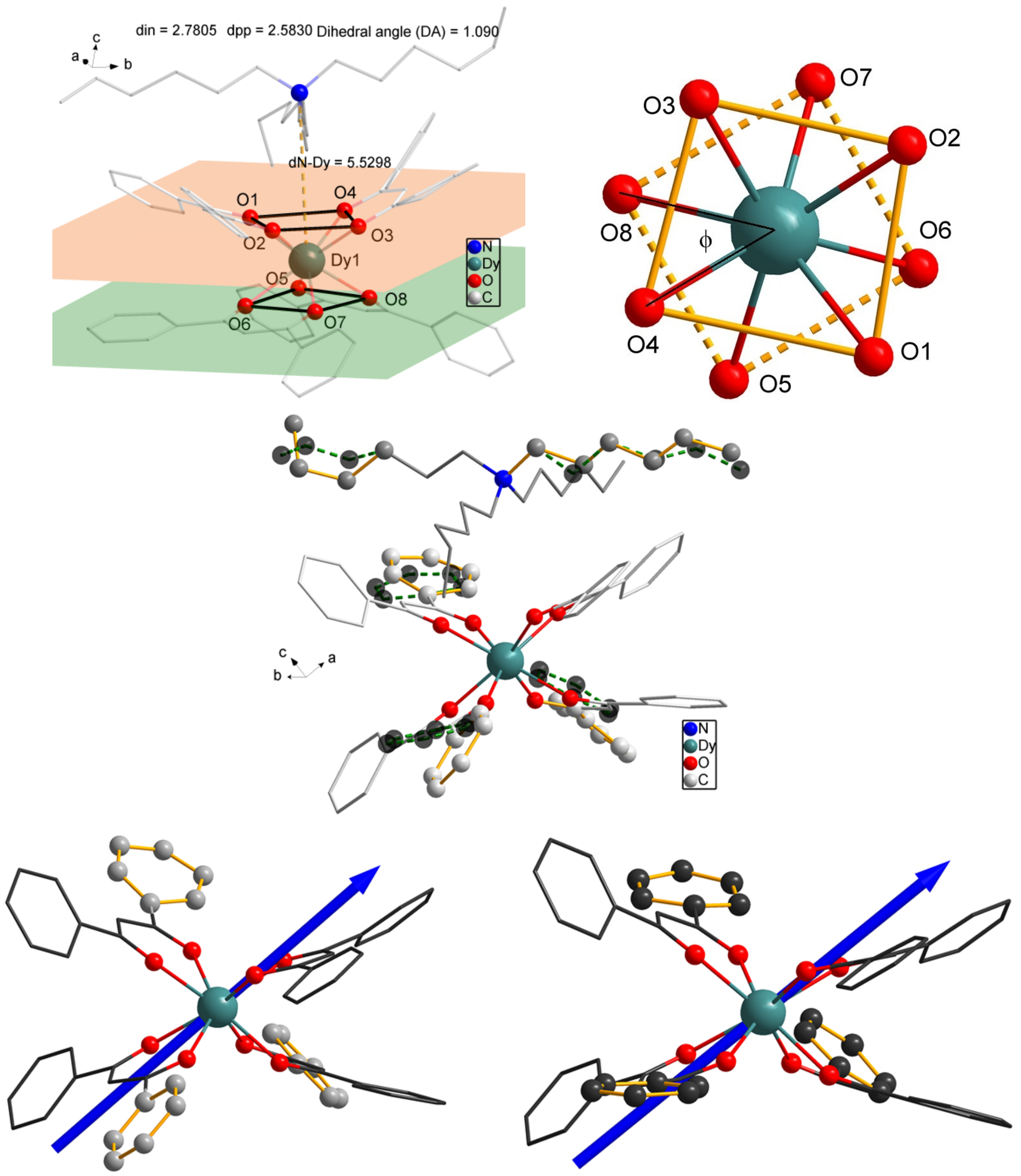

Fig. S1 (Top left) The coordination geometry around Dy(III) ion (upper plane (pink) consists of O1, O2, O3 and O4, lower plane (green) consist of O5, O6, O7 and O8); Top right: Perspective showing the ϕ structural features; middle: the structure of **1** and the black ball represent the disorder atoms, we named the light grey part as **1**a and the disorder black ball part as **1**b; Bottom left (**1**a) and right (**1**b) shows the two disorder structures and their calculated direction of magnetic easy axial respectively (blue arrow), the calculated g tensor are listed in Table S3 and S4.

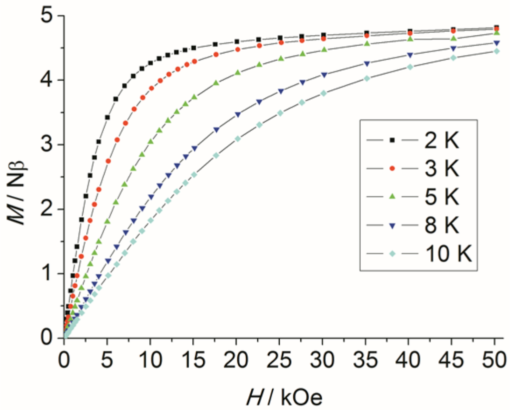

Fig. S2 The field dependence of magnetization at 2, 3, 5, 8 and 10 K.

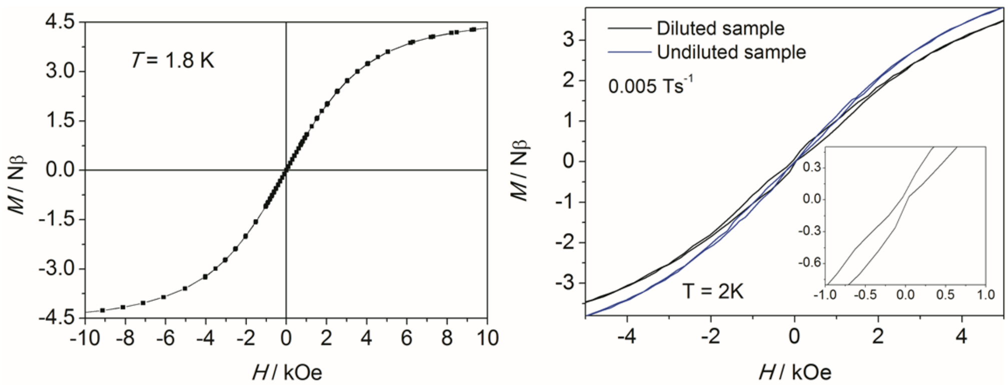

Fig. S3 Magnetization (*M*) *vs.* applied dc field (*H*) on a Quantum Design MPMS XL-5 SQUID magnetometer (left) and a Quantum Design PPMS magnetometer with a sweep rate of 0.005 $T \cdot s^{-1}$ (right) at 2 K. Inset: Zoomed-in section of the hysteresis loops showing an small opening for a diluted sample.

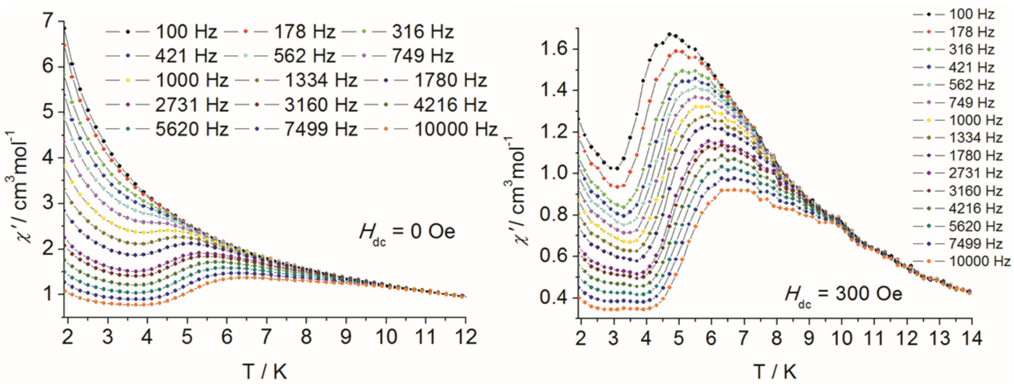

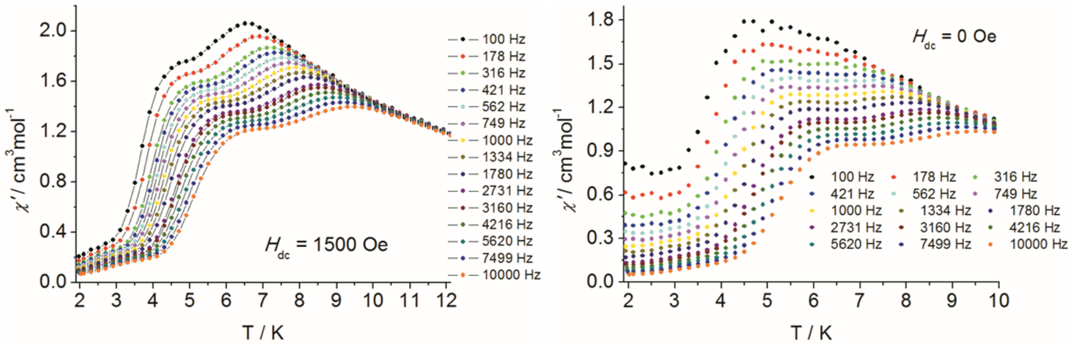

Fig. S4 The temperature dependence of the in-phase (χ') ac susceptibility component under zero (top left), 300 (top right), 1500 Oe (bottom left) dc fields for **1** and under zero dc field for diluted sample [Hex][$Y_{0.95}Dy_{0.05}(DBM)_4$] (bottom right).

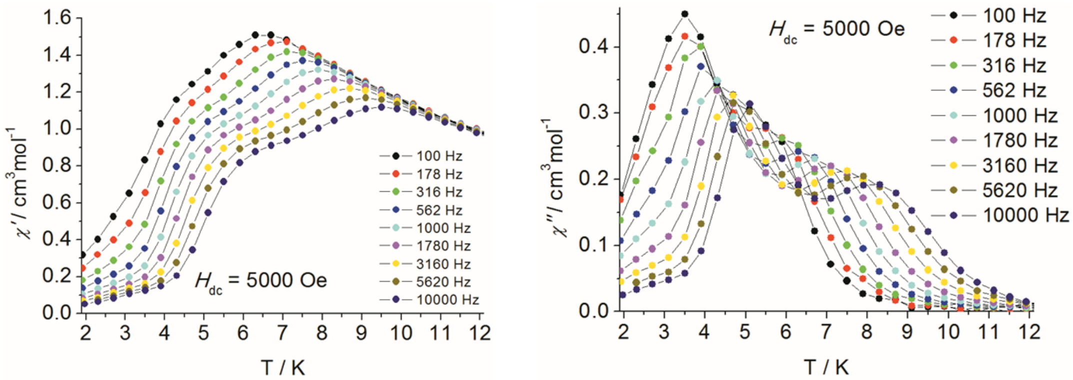

Fig. S5 The temperature dependence of the in-phase (χ', left) and the out-of-phase (χ'', right) ac susceptibility component under 5000 Oe dc field for **1**.

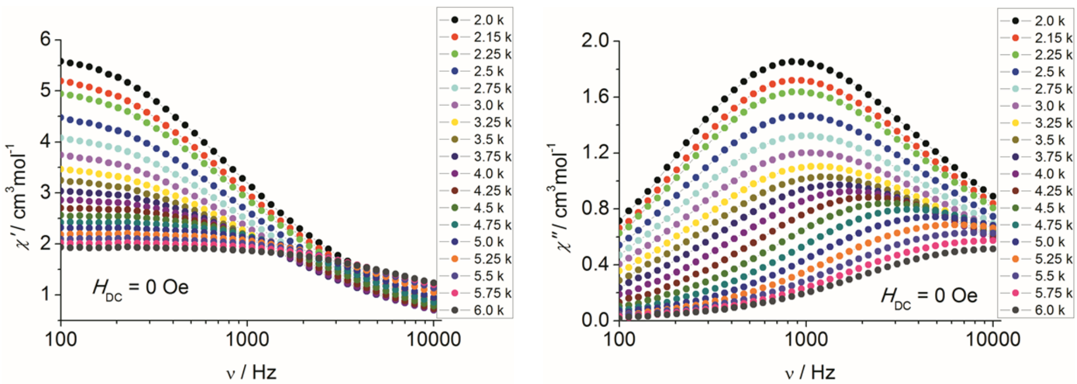

Fig. S6 Frequency dependence of the in-phase (χ', left) and the out-of-phase (χ'', right) ac susceptibility component under zero dc fields for **1**.

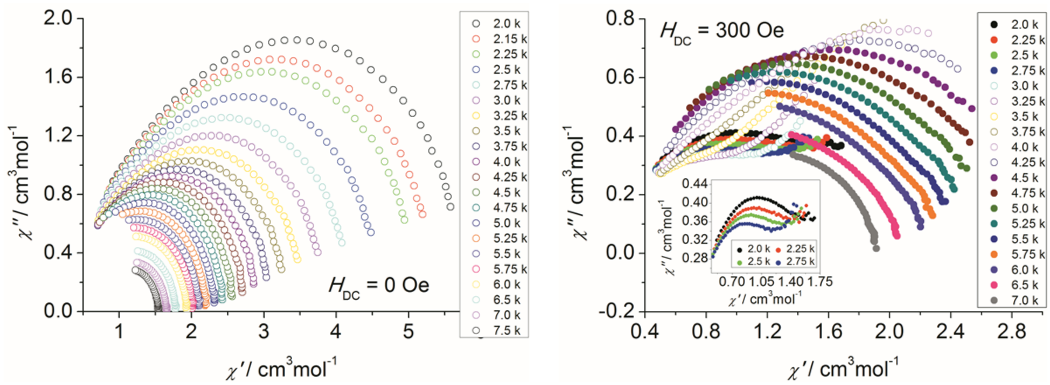

Fig. S7 The cole-cole plot for undiluted **1** under zero dc field (left) and 300 Oe field (right).

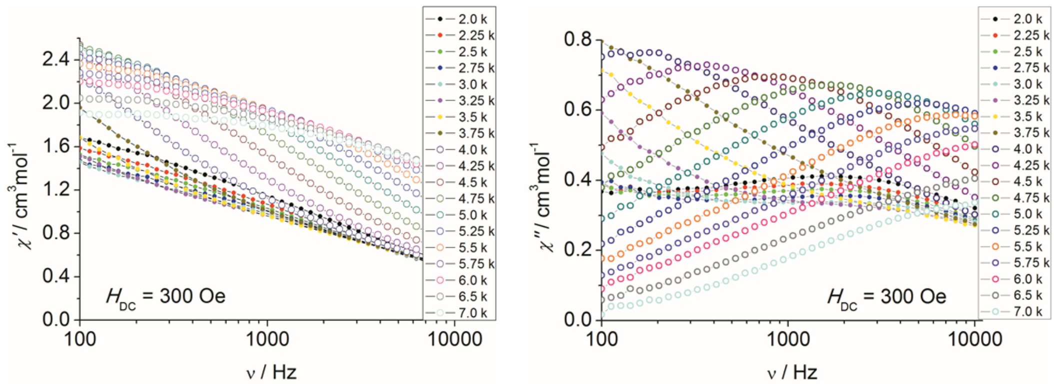

Fig. S8 Frequency dependence of the in-phase (χ', left) and the out-of-phase (χ'', right) ac susceptibility component under 300 Oe dc fields for **1**.

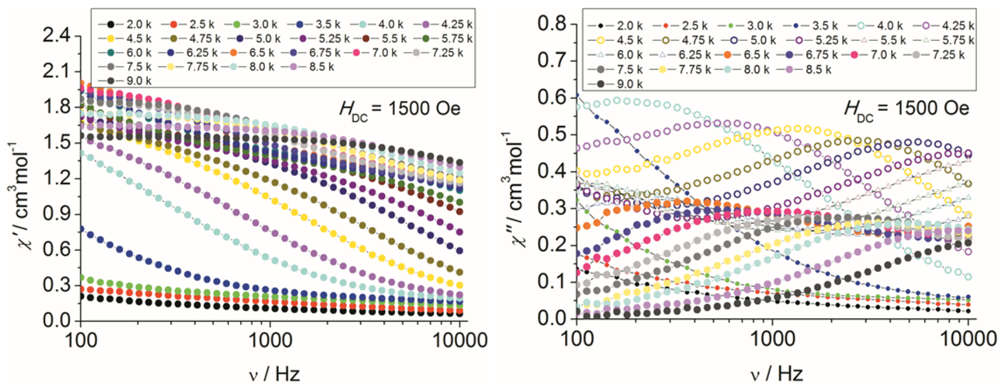

Fig. S9 Frequency dependence of the in-phase (χ', left) and the out-of-phase (χ'', right) ac susceptibility component under 1500 Oe dc fields for **1**.

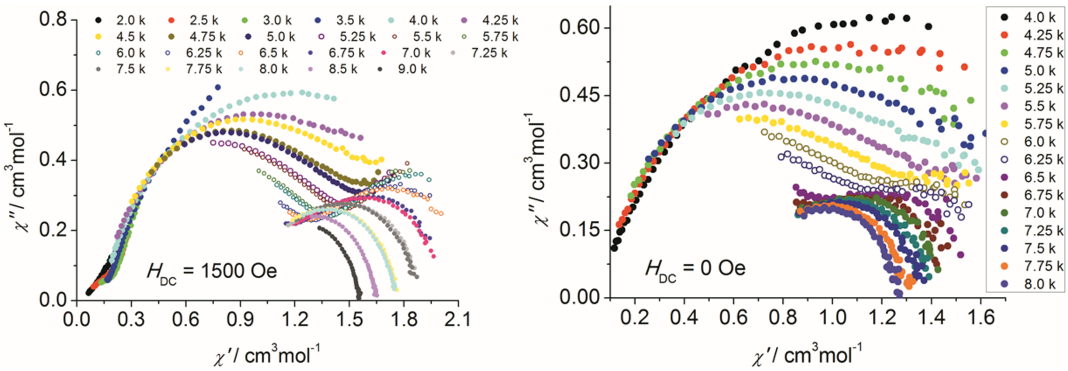

Fig. S10 The cole-cole plot for undiluted **1** under 1500 Oe (left) and diluted sample [HexN][$Y_{0.95}Dy_{0.05}(DBM)_4$] under zero Oe dc field (right).

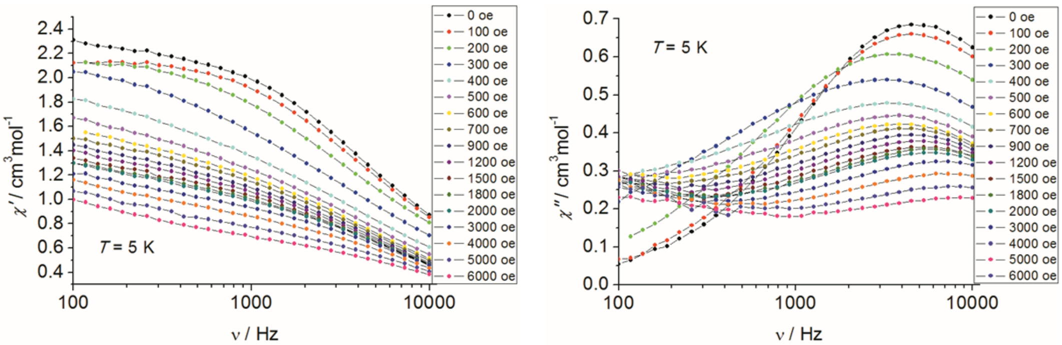

Fig. S11 Frequency dependence of the in-phase (χ', left) and the out-of-phase (χ'', right) ac susceptibility component at 5 K under different dc fields for **1**.

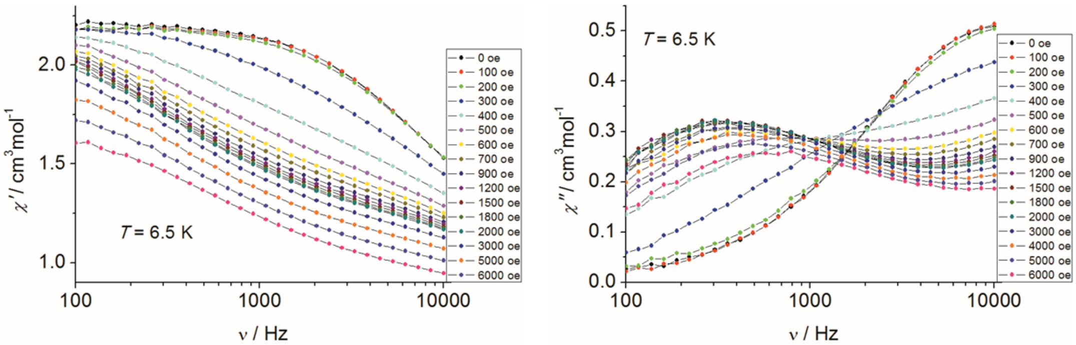

Fig. S12 Frequency dependence of the in-phase (χ', left) and the out-of-phase (χ'', right) ac susceptibility component at 6.5 K under different dc fields for **1**.

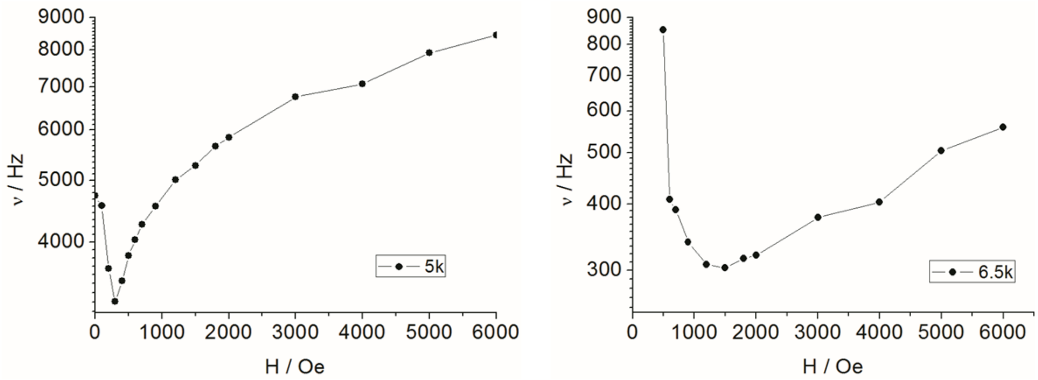

Fig. S13 Field dependence of the characteristic frequency as a function of the applied dc field for **1** at 5 K (left) and 6.5 K(right).

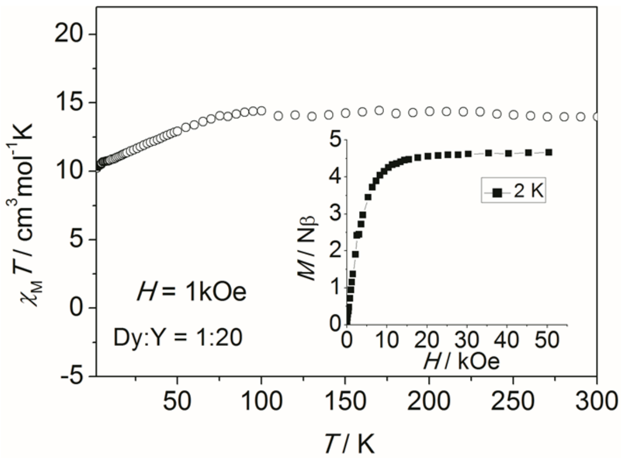

Fig. S14 Temperature dependence of $\chi_M T$ measured at 1 kOe for [Hex][$Y_{0.95}Dy_{0.05}(DBM)_4$], (inset: The field dependence of magnetization at 2 K).

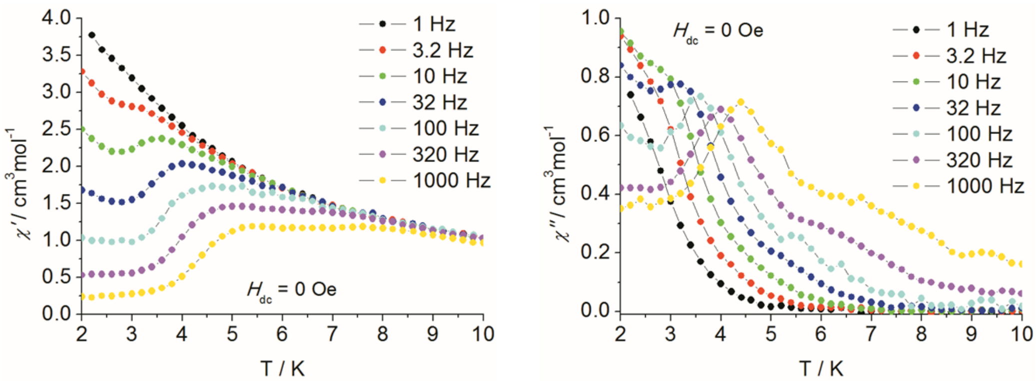

Fig. S15 The temperature dependence of the in-phase (χ', left) and the out-of-phase (χ'', right) ac susceptibility component under zero dc fields for [Hex][$Y_{0.95}Dy_{0.05}(DBM)_4$].

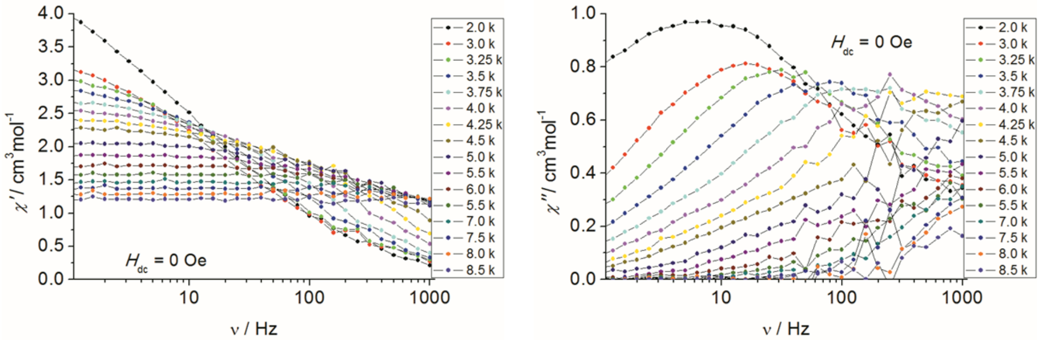

Fig. S16 Frequency dependence of the in-phase (χ', left) and the out-of-phase (χ'', right) ac susceptibility component under zero dc fields for [Hex][$Y_{0.95}Dy_{0.05}(DBM)_4$].

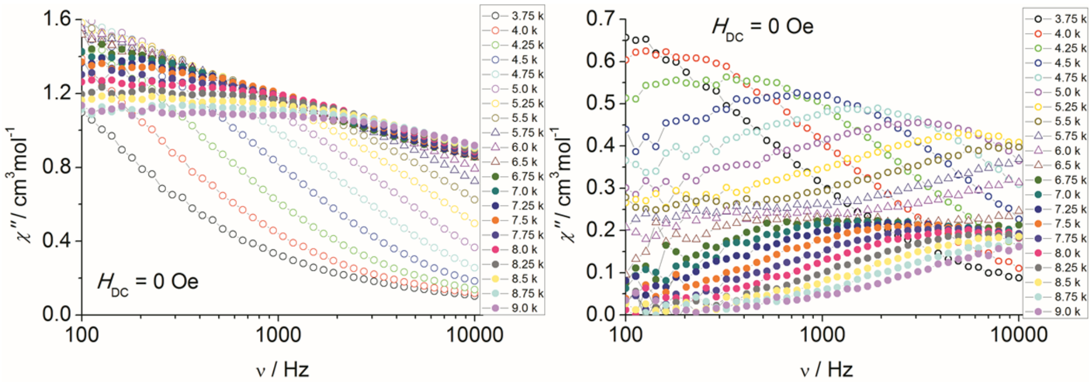

Fig. S17 Frequency dependence of the in-phase (χ', left) and the out-of-phase (χ'', right) ac susceptibility at frequencies from 100 to 10000 Hz under zero dc fields for [HexN][$Y_{0.95}Dy_{0.05}(DBM)_4$].

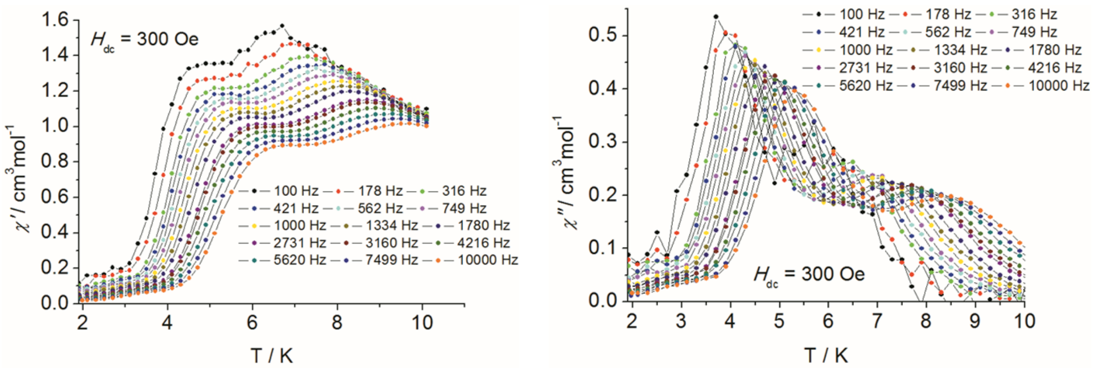

Fig. S 18 The temperature dependence of the in-phase (χ', left) and the out-of-phase (χ'', right) ac susceptibility at frequencies from 100 to 10000 Hz under 300 Oe dc fields for [Hex][$Y_{0.95}Dy_{0.05}(DBM)_4$].

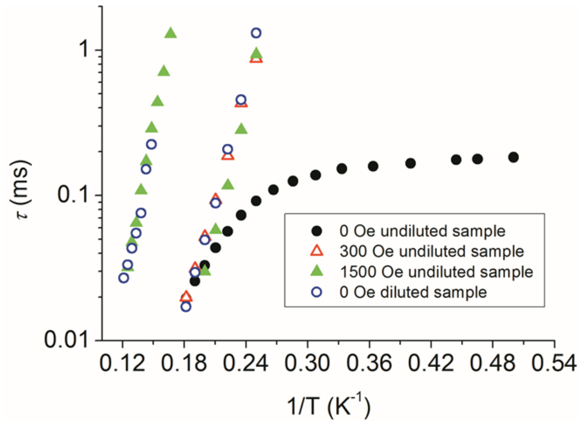

Fig. S 19 Plots of τ vs T^{-1} at H_{dc} = 0, 300 and 1500 Oe for the undiluted and diluted samples.

Table S1 The effective relaxation energy barriers U_{eff} and pre-exponential factor τ_0 from fitting Arrhenius law.

dc field (Oe)	Low temperature U_{eff} = ΔE/k and τ_0	High temperature U_{eff} = ΔE/k and τ_0
0	27.7 and 1.3×10^{-7}	
300	56.6 and 6.6×10^{-10}	
1500	68.1 and 3.4×10^{-11}	88.0 and 5.0×10^{-10}
0 (Diluted sample, 100-10000 Hz)	63.8 and 1.6×10^{-10}	79.8 and 1.5×10^{-9}

Table S2 The calculated effective relaxation energy barriers U_{eff}

Complex	Calculated ΔE	ΔE_{1b}-ΔE_{1a}
1a	57 cm^{-1} (80 K)	22 K
1b	73 cm^{-1} (102 K)	

Table S3 Calculated g tensor and energy spectrum of compound **1**a

g_X	g_Y	g_Z
0.0354	0.0754	19.462

Energy (au) of 16 lowest states		Relative Energy (eV)	Relative Energy (cm^{-1})
1	-42.78245884	0.000000	0.000
2	-42.78245884	0.000000	0.000
3	-42.78219888	0.007074	57.056
4	-42.78219888	0.007074	57.056
5	-42.78191826	0.014710	118.644
6	-42.78191826	0.014710	118.644
7	-42.78176301	0.018935	152.718
8	-42.78176301	0.018935	152.718
9	-42.78168776	0.020982	169.233
10	-42.78168776	0.020982	169.233
11	-42.78145278	0.027376	220.805
12	-42.78145278	0.027376	220.805
13	-42.78118353	0.034703	279.899
14	-42.78118353	0.034703	279.899
15	-42.78059218	0.050795	409.686
16	-42.78059218	0.050795	409.686

Table S4 Calculated g tensor and energy spectrum of compound **1**b

g_X	g_Y	g_Z
0.0161	0.0308	19.5069

Energy (au) of 16 lowest states		Relative Energy (eV)	Relative Energy (cm^{-1})
1	-42.83185378	0.000000	0.000
2	-42.83185378	0.000000	0.000
3	-42.83152142	0.009044	72.946
4	-42.83152142	0.009044	72.946
5	-42.83127050	0.015872	128.016
6	-42.83127050	0.015872	128.016
7	-42.83107753	0.021123	170.367
8	-42.83107753	0.021123	170.367
9	-42.83099983	0.023237	187.420
10	-42.83099983	0.023237	187.420
11	-42.83076679	0.029578	238.566
12	-42.83076679	0.029578	238.566
13	-42.83046821	0.037703	304.098
14	-42.83046821	0.037703	304.098
15	-42.83004205	0.049300	397.629
16	-42.83004205	0.049300	397.629